Cobalt anti-MXenes as Promising Anode Materials for Sodium-ion Batteries

Subhadeep Banerjee,[1,2] Kalpak Gosh,[1,3] Sandeep K Reddy,[5] and Sharma S. R. K. C. Yamijala[1,2,3,4,*]

1. Department of Chemistry, Indian Institute of Technology Madras, Chennai, 600036 India.
2. Centre for Atomistic Modelling and Materials Design, Indian Institute of Technology Madras, Chennai 600036, India.
3. Centre for Quantum Information, Communication, and Computing, Indian Institute of Technology Madras, Chennai 600036, India.
4. Centre for Molecular Materials and Functions, Indian Institute of Technology Madras, Chennai 600036, India.
5. Centre for Computational and Data Science, Indian Institute of Technology Kharagpur, Kharagpur, West Bengal, 721302 India.
* yamijala@iitm.ac.in

Abstract

The current electric vehicle market is entirely dominated by lithium-ion batteries (LIBs). However, due to the limited and unequal distribution of LIB raw materials on earth, there is a continuous effort to design alternate storage devices. Among the alternatives to LIBs, sodium-ion batteries (NIBs) are at the forefront because sodium resources are ubiquitous worldwide and virtually inexhaustible. However, one of the major drawbacks of the NIBs is their low specific charge capacity. Since the specific charge capacity of a cell can be improved by increasing the specific charge capacity of the anode material, there is a constant effort to find suitable anode materials. Recent studies suggested that cobalt-boride (CoB) anti-MXene material (a newly discovered two-dimensional material) can yield superior specific charge capacities for LIBs than traditional graphite-based anodes. Inspired by these findings, in this work, we considered six cobalt-based anti-MXene materials (Co-anti-MXenes), namely, CoAs, CoB, CoP, CoS, CoSe, and CoSi, and examined their competency as anode materials for NIBs. Our findings suggest that Co-anti-MXenes possess superior specific charge capacities (~ 390–590 mAh/g) than many well-studied anode materials like MoS_2 (146 mAh/g), Cr_2C (276 mAh/g), expanded graphite (284 mAh/g), etc. Moreover, their greater affinity (-0.55 to -1.16 eV) to Na atoms, along with reasonably small diffusion energy barriers (0.32 to 0.59 eV) and low average sodiation voltages (0.2 to 0.64 V), suggest that these Co-anti-MXenes can serve as excellent anode materials for NIBs.

Introduction

The recent Russia-Ukraine war gives us a glimpse of how the world would quickly go into an energy crisis when fossil fuels become scarce. Apart from being finite and nonrenewable, fossil fuels also alter our climate and will lead to a 0.6 % increment in global warming from 2017 to 2050.[1] As such, global energy consumption should shift from fossil fuels to renewable and clean energy sources as quickly as possible. Also, since the energy supply from renewable energy resources (like wind, solar, geothermal, etc.) depends on various factors (such as time, weather conditions, geographical location, etc.), the energy generated from these resources needs to be stored. One of the efficient ways to store energy is through electrochemical cells, and among various choices, rechargeable lithium-ion batteries (LIBs) are at the forefront due to their high energy efficiency and low maintenance cost.[2–5] However, the major drawback of LIBs is the unequal distribution of their raw materials over the globe and the limited availability of lithium in the earth's crust, leading to geopolitical tensions.

While there are several alternatives to LIBs,[6–12] sodium-ion batteries (NIBs) have gained considerable attention since sodium is abundant in the earth's crust (sixth most abundant element). Its resources are distributed nearly equally throughout the world, and it has a lower cost of extraction.[13] Further, since Li and Na are located in the same group of the periodic table and since they both possess only one electron in their valence shell, it is expected that the nature of the electrochemical half-cell reactions would be the same. Also, the reduction potential of sodium is just 0.33 V above the lithium ($E^0_{Na+/Na}$ = -2.71 V and $E^0_{Li+/Li}$ = -3.04 V). However, the larger ionic radius of the Na^+ ion (1.02 Å) than the Li^+ ion (0.76 Å) makes it difficult to insert or extract the sodium ions from the host material, affecting the mass transport, storage, and overall kinetics.[14,15] Therefore, finding suitable electrode materials with superior electrochemical properties is crucial for making NIBs with commercial applications. Several recent studies have made progress on both cathode and anode materials of NIBs.[16–19] However, significant efforts are still required to find new anode materials with high specific charge capacities and lower redox potentials (closer to the Na^+/Na redox couple).

In a recent study,[20] Jinxing et al. discovered a new class of materials called anti-MXenes, with promising electrochemical and catalytic applications. They studied about 79 anti-MXene materials and found that around 24 anti-MXene materials are stable. Moreover, they found two of these materials, CoB and FeB, suitable for LIB applications with high specific charge capacities (1099.44 and 1135.77 $mAhg^{-1}$, respectively). Inspired by these findings, in this work, we have explored six cobalt (Co) containing anti-MXene materials, namely, CoAs, CoB, CoP, CoS, CoSe, and CoSi, and inspected their ability to serve as anode materials in sodium-ion batteries (NIBs). Using density functional theory calculations, we computed various physical and electrochemical properties such as specific charge capacity, open-circuit voltage, Na-atom binding energy, Na-ion diffusion barrier, etc. Our calculations suggested that sodium has greater binding energy (-0.55 to -1.16 eV) and reasonably low diffusion energy barriers (0.32 to 0.59 eV) on Co-anti-MXenes. Also, Co-anti-MXenes possess low average sodiation voltages (0.2 to 0.64 V) and high specific charge capacities (~ 390–590 $mAhg^{-1}$), which are desirable properties of good anode material for NIBs. Interestingly, specific charge capacities of Co-anti-MXenes are

superior than many well-established anode materials like graphite (<35 $mAhg^{-1}$),[21] expanded graphite (284 $mAhg^{-1}$),[15] MoS_2 (146 $mAhg^{-1}$),[22] and various M_2C MXenes [M = Nb (219 $mAhg^{-1}$), V (335 $mAhg^{-1}$), Ti (348 $mAhg^{-1}$)],[23] etc. Together, these properties suggest that the Co-anti-MXenes fit as excellent anode materials for NIBs.

Computational Details

All electronic structure calculations were performed using the density functional theory (DFT) as implemented in the Vienna ab initio simulation package (VASP).[24] The projected augmented wave (PAW) pseudopotential method was used to account for the core electrons, and valence electrons were represented with a plane-wave basis with a cut-off of 450 eV.[25] For the exchange-correlation interaction, the generalized gradient approximation (GGA) is used within the Perdew-Burke-Ernzerhof (PBE) scheme.[26,27] Dispersion interactions were included using the DFT-D3 method along with the Becke-Jonson damping.[28] The lattice constant along the z-direction was fixed at 40 Å to avoid any spurious interactions between the periodic images. Except for the migration energy barrier (MEB) and charge-density difference (CDDs) calculations, all simulations were performed with a 1×1 unit cell. To sample the Brillouin zone, a Monkhrost-Pack[29] k-mesh of 12×12×1 and 25×25×1 were used for the structural relaxation and density of states (DOS) calculations, respectively. The climbing-image nudged elastic band (CI-NEB)[30] method was used to find the MEB for the diffusion of a sodium metal atom on the Co-anti-MXenes. For these calculations, a 3×3 supercell along with a 4×4×1 k-mesh was considered. The force and energy convergence criteria were set to 0.02 eV/Å and 10^{-5} eV, respectively. Thermal stability of these materials was examined by performing *ab initio* molecular dynamics (AIMD) simulations in the NVT (canonical) ensemble for a 15 ps duration with a 1 fs timestep. The temperature was maintained at 300 K using the Nosé–Hoover thermostat. VASPKIT and pymatgen were used to obtain the relevant post-processing data, and in-house python scripts were used to plot the band structure, density of states, etc.[31,32] VESTA was used to visualize the optimized structures, electron localization functions, and charge-density difference maps.[33]

Results and Discussion

Stability and Structural Information

Since earlier work by Chen group[20] has already proved that the Co-anti-MXenes are quite stable, here, we only discuss their structural information briefly. **Figures 1a** and **1b** depict the top and side views of the optimized structure of CoS anti-MXene, respectively. The optimized geometries of all other anti-MXenes are shown in **Figure S1**. As shown in these figures, in anti-MXenes, the metal atomic layer is sandwiched between two non-metal atomic layers, an arrangement that is exactly opposite to the arrangement in MXenes, and hence the name anti-MXenes. The calculated layer thickness and bond distances of the Co-anti-MXenes are given in **Table S1**, and they are in excellent agreement with the earlier study,[20] validating our

calculations. The electron localization function (ELF) plots (**Figures 1d, 1e,** and **S2**) show that the electrons are primarily localized on the non-metal atoms, indicating an ionic-type interaction between the elements Co and X (=As, B, P, S, Se, and Si), which stabilizes these systems.

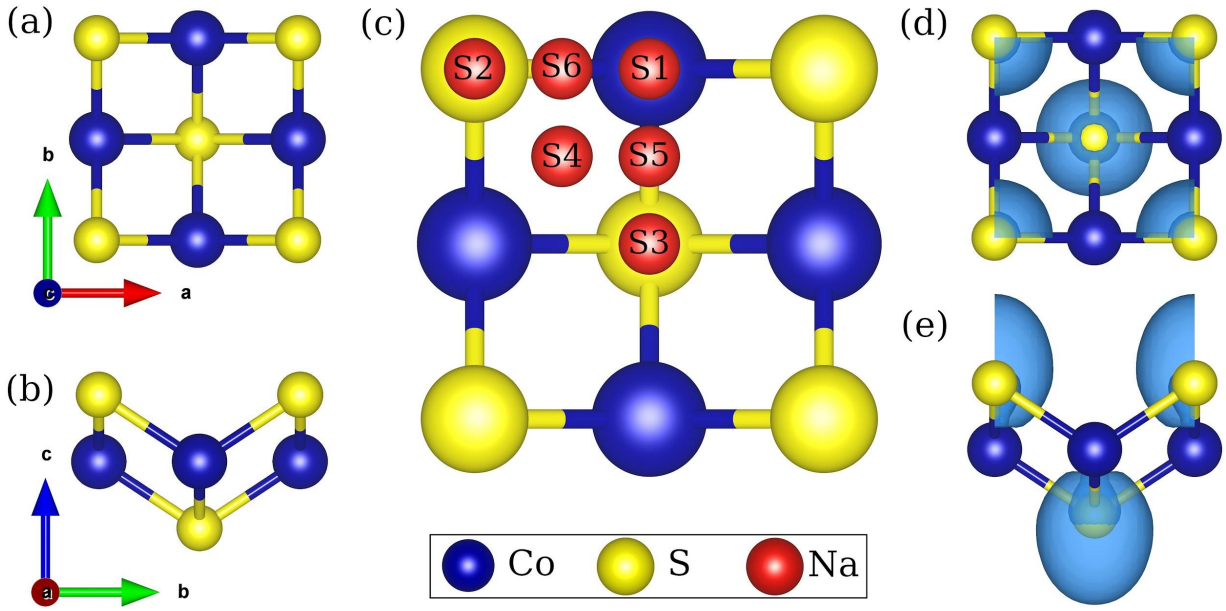

Figure 1. (a) Top and (b) side views of the optimized CoS structure. Each Co (S) atom is bonded to four S (Co) atoms. (c) various Na atom adsorption sites (depicted as S1-S6, see text for more details) on a CoS anti-MXene that we considered in this study, and (d) top and (e) side views of the electron localization function (ELF) plot of the CoS structure. Clearly, the electrons are localized on the S atom, indicating an ionic-type interaction between the elements Co and S. An isosurface value of 0.5 e/ Å ^{3} is used for the ELF plot.

In **Figure 2**, we presented the band structure and projected density of states (PDOS) of all the anti-MXenes. The presence of a finite density of states near the Fermi-level in the PDOS plots indicates that these systems are metallic. Furthermore, as evident from the PDOS plots, the metallic character of the anti-MXenes is primarily due to the cobalt atoms (more specifically, due to the Co d-orbitals, **Figure S3**). Since electrons have to flow from the anodic compartment to the external load during the discharging process of a battery, a metallic electrode (i. e., a good electrical conductor) is beneficial for the electrochemical cell. As such, all the six Co-anti-MXenes have the potential to be used as anodes. To further check their relevance as anodes for Na-ion batteries, we have calculated a few crucial properties such as Na atom adsorption energy, Na atom migration energy barrier, theoretical specific charge capacity, sodiation voltage, etc. First, we will discuss the adsorption properties of Na on these six anti-MXenes.

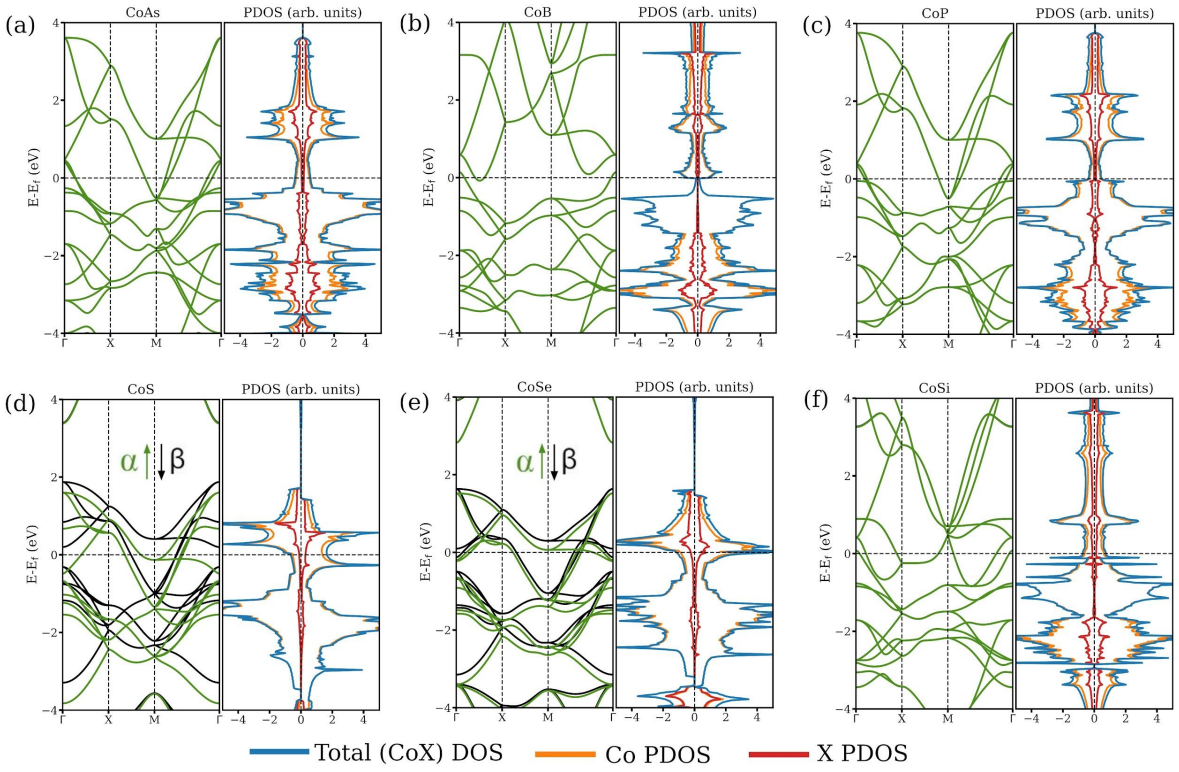

Figure 2. Band structure and projected density of states (PDOS) of (a) CoAs (b) CoB (c) CoP (d) CoS (e) CoSe and (f) CoSi. Except for CoS and CoSe, all systems possess spin-unpolarized ground states. All the anti-MXenes have a finite DOS near the Fermi level indicating that they are metallic and have the potential to be used as electrodes. States across the Fermi-level have a major contribution from the cobalt atoms, indicating their contribution to the metallicity.

Preferential Adsorption of a Na Atom on CoX Surfaces

Figure 1c depicts the six different possible adsorption sites for the Na atom on the CoX surfaces. These six sites can be identified based on the Na atom's position with respect to the Co (middle layer) and X atoms (top and bottom layers, see **Figure 1b**) of the anti-MXene; S1: on top of the Co atom, S2: on top of the top-layer X atom, S3: on top of the bottom-layer X atom, S4: on top of the hollow position of Co_2X_2 square, S5: on top of the Co and bottom-layer X atom's bond, and S6: on top of the Co and top layer X atom's bond. Among these six possible sites, we find that the Na adsorption is stable (i.e., with negative adsorption energy) only at the S1, S2, and S3 sites on any CoX surface. The adsorption energy of a single sodium atom on a pristine CoX surface is calculated as $E_{ads} = E_{Na+CoX} - E_{CoX} - E_{Na}$, where E_{Na+CoX} is the energy of the CoX surface along with the adsorbed Na atom, E_{CoX} is the energy of the pristine CoX surface, and E_{Na} is the energy of a single sodium atom in its bulk bcc lattice.

Table 1. Single Na atom adsorption onto Co-anti-MXenes at S1, S2, and S3 sites.

System	Ads. Energy (eV)			Na - CoX surface distance (Å)			Charge on the Na atom		
	S1	S2	S3	S1	S2	S3	S1	S2	S3
CoAs	-0.277	0.103	***-0.702***	2.256	2.817	***1.259***	0.498	0.280	***0.732***
CoB	-0.683	-0.375	***-1.101***	2.023	2.475	***1.528***	0.553	0.396	***0.674***
CoP	-0.470	-0.218	***-0.939***	2.181	2.793	***1.280***	0.507	0.294	***0.740***
CoS	-0.241	-0.047	***-0.570***	2.107	2.747	***1.243***	0.479	0.269	***0.712***
CoSe	-0.210	-0.031	***-0.548***	2.271	2.869	***1.311***	0.448	0.236	***0.716***
CoSi	-0.507	-0.109	***-1.156***	2.124	2.860	***1.241***	0.600	0.293	***0.748***

Interestingly, as shown in **Table 1**, the stability order of a Na atom on all the CoX surfaces is S3 > S1 > S2, i.e., a Na atom adsorbs strongly at the S3 site irrespective of the CoX surface. Moreover, this stability order is consistent with the Na atom's height from the CoX surface: S3 < S1 < S2, where, at lower heights, a Na atom adsorbs strongly onto a CoX surface (due to the greater bonding between the Na atom and the surface). For example, on the CoS surface, the optimized Na atom adsorption heights are: S3 (1.243 Å) < S1 (2.107 Å) < S2 (2.747 Å). The greater adsorption strength at the S3 site primarily stems from the fact that at an S3 site a Na atom can interact simultaneously with four non-metal (X) atoms. In contrast, at the S1 and S2 sites, that number reduces to two and one, respectively (see **Figure 3**).

The differences in the interaction between the Na atom and non-metal atoms at the S1, S2, and S3 sites of the CoX surfaces can be explicitly noted in the charge-density difference plots (CDDs) and Bader charges analysis. The CDDs are calculated as $\Delta\rho(NaCoX) = \rho(NaCoX) - \rho(CoX) - \rho(Na)$, where $\rho(NaCoX)$, $\rho(CoX)$, and $\rho(Na)$ are the total charge densities of a 3×3-CoX surface with a Na atom adsorbed onto it, a pristine 3×3-CoX surface, and a single Na atom in the same supercell. While calculating ρ(CoX) and ρ(Na), the same coordinate space of ρ(NaCoX) was used. **Figure 3** depicts the CDDs of a CoS system with a single Na atom adsorbed at S1, S2, and S3 sites. In all three cases, there is a charge transfer from the Na atom to the top-layer sulfur atoms. However, there is an apparent difference in how the electrons are shared between the Na atom and sulfur atoms. At the S3 site, the transferred electrons are shared with four sulfur atoms making it the most favorable stable site for Na atom adsorption. At the S1 and S2 sites, electrons are shared only with two and one sulfur atom, respectively. Moreover, as shown in **Table 1**, the Na atom donates a greater charge (to the non-metal atoms) at the S3 site than at the S1 and S2 sites. Indeed, our Bader-charge analysis on the CoS system shows that the amount of charge transfer from the Na atom follows the adsorption stability trend, i.e., S3 > S1 > S2. Similar behavior is observed in all other CoX anti-MXenes (see **Figure S4** for the CDDs of other systems), where the electrons transferred from the Na atom are shared with four non-metal (X) atoms. Thus, the greater stability of the Na atom at the S3 site is due to its strong ionic interaction with multiple non-metal atoms.

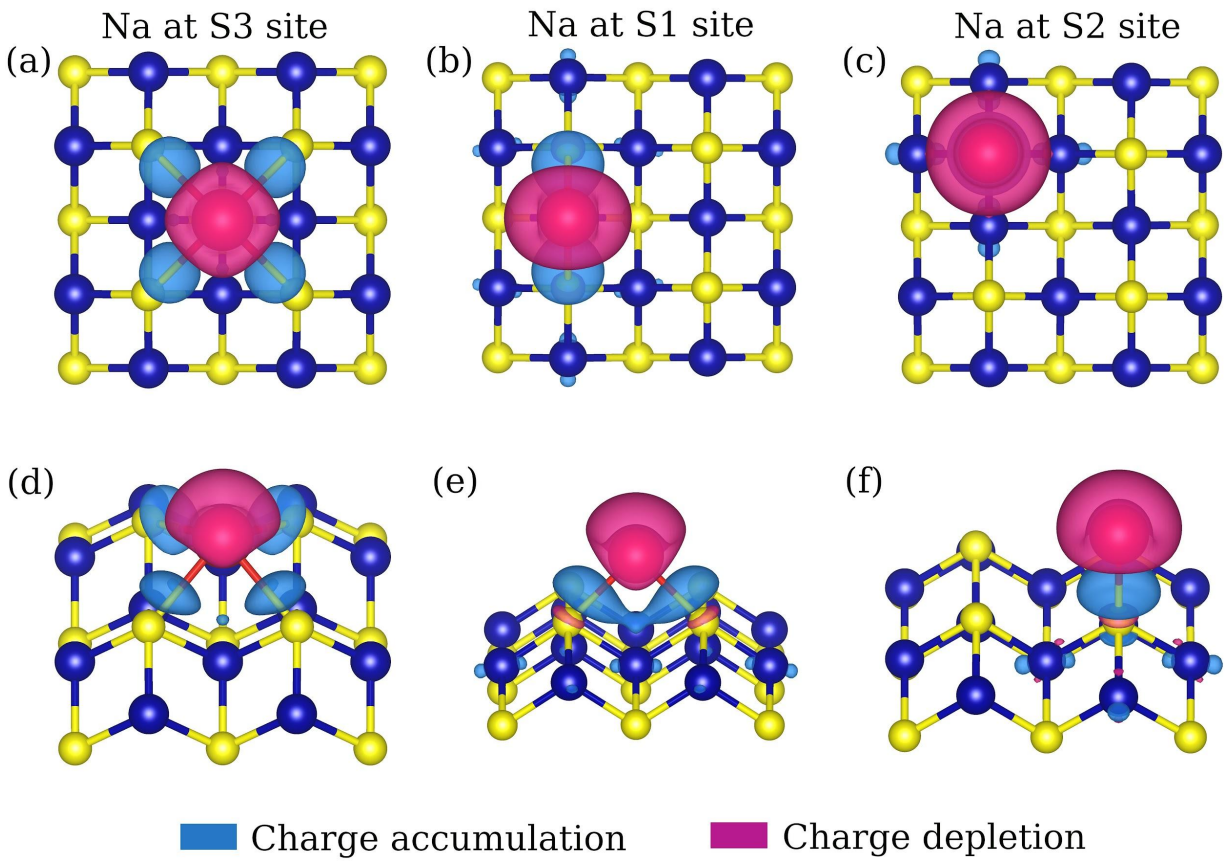

Figure 3. Top and side-views of the charge-density difference maps (CDDs) of a CoS system with Na atom adsorbed at S3 (a,d), S1 (b,e), and S2 (c,f) sites, respectively. The magenta (sky-blue) color depicts the charge depletion (accumulation). It is apparent that the Na atom interacts with four, two, and one sulfur atoms when it is adsorbed at the S3, S1, and S2 sites of the CoS surface, respectively. An isosurface value of 0.002 e/Å^3 is used in all plots. The side views are slightly tilted to show the Na-S bonds. See **Figure S4** for the CDDs of other systems.

The adsorption energy values of a single Na atom at the S3 site of all the Co-anti-MXenes are given in **Table 1**. They lie in the energy range of -0.55 eV to -1.16 eV, suggesting strong physisorption of the Na atom on Co-anti-MXenes.[34] A few materials with such strong Na atom adsorption energies (predicted using DFT) and that were **experimentally** used as anode materials in NIBs include MXenes like $Ti_3C_2O_2$ (-0.83 eV),[35,36] V_2CO_2 (-0.88 eV),[35,37] $Hf_3C_2F_2$ (-0.91 eV),[35,38] and other two-dimensional materials like rutile TiO_2 (-0.61 eV),[39,40] MoS_2 (-0.77 eV)[41,42] etc are comparable with the adsorption energy values of Co-anti-MXene materials. Possessing such a strong physisorption value is beneficial for an anode (here, CoX) since it prevents the dendrite formation while loading multiple Na atoms onto the anode surfaces. Also, among functionalized MXene materials, superior specific charge capacities were observed for materials with greater adsorption strengths,[35] hinting that some of the anti-MXenes considered in this work could possess higher specific charge capacities. Apart from binding the metal atoms firmly, a promising anode material should also allow them to diffuse quickly on its

surface during the charge/discharge cycles. Below, we have presented the diffusion energy barriers for a sodium atom on all the Co-anti-MXenes.

Migration Energy Barrier

At equilibrium, since the metal atoms are expected to sit at the most stable sites of the Co-anti-MXene surface, the diffusion/migration energy barriers (MEBs) are calculated by moving a sodium atom from one stable site (here, S3) to the other along different paths. **Figure 4a** shows three possible paths considered in this study on a CoS surface. Here, path-1 corresponds to the Na atom movement along the 'a'-direction of the lattice, i.e., from S3→S5→S1→S5→S3. In paths 2 and 3, the Na atom moves at an angle to both a and b-directions of the lattice. In path-2, the Na atom moves along S3→S6→S3, and in path-3, it moves along S3→S4→S2→S4→S3. To find the MEBs along each of these paths, we considered a 3×3 supercell and performed the climbing-image nudged elastic band (CI-NEB) calculations. Among the three paths, as shown in **Figure 4b**, the MEB value is the least along path-1 (0.402 eV) and highest along path-3 (0.86 eV). We could not estimate the MEB value along path-2 from the CI-NEB calculations since the images along path-2 always converged to path-1. As such, we chose an alternate way to estimate the MEB value along path-2; we calculated the adsorption energy of the Na atom at the S6 site by fixing its 'x' and 'y' coordinates (i.e., only the z-coordinate of the Na atom is allowed to relax during the optimization). Through these calculations, we find that Na at the S6 site is ~ 0.76 eV higher in energy than at the S3 site. Thus, the MEB along path-2 is expected to be at least 0.3 eV higher in energy than the MEB along path-1.

To understand the lower MEB along path-1, we plotted the electron localization function (**Figure 4c**) along the (001) plane of the CoS surface. Since sodium tends to lose its valence electron (i.e., it is electron-rich), it would encounter a high (low) barrier when it diffuses through regions of high (low) electron density. As shown in the ELF plot, since a sodium atom along path-1 (path-3) encounters regions of low (high) electron density at S1 (S2) sites, it experiences a low (high) barrier for diffusion. This result can also be understood from the CDD plots (cf. **Figure 3**). As explained earlier, a Na atom shares its electrons with four, two, and one sulfur atoms when it is adsorbed at the S3, S1, and S2 sites, respectively, and its stability is more when it shares its electrons with a more number of non-metal atoms. Now, when a Na atom moves along the path-1, it first shares its electrons with four sulfur atoms (at S3), next with two sulfur atoms (at S1), and finally again with four sulfur atoms (at the next S3). On the other hand, when it moves along path-3, it can only share its electrons with a single sulfur atom (at S2), and thus a higher barrier for its diffusion. As such, path-1 is the most favorable path for the Na atom's diffusion since a Na atom can share its electrons with a larger number of non-metal atoms along this path (**Figure 3**), and also since it is an electron-deficient path (**Figure 4c**).

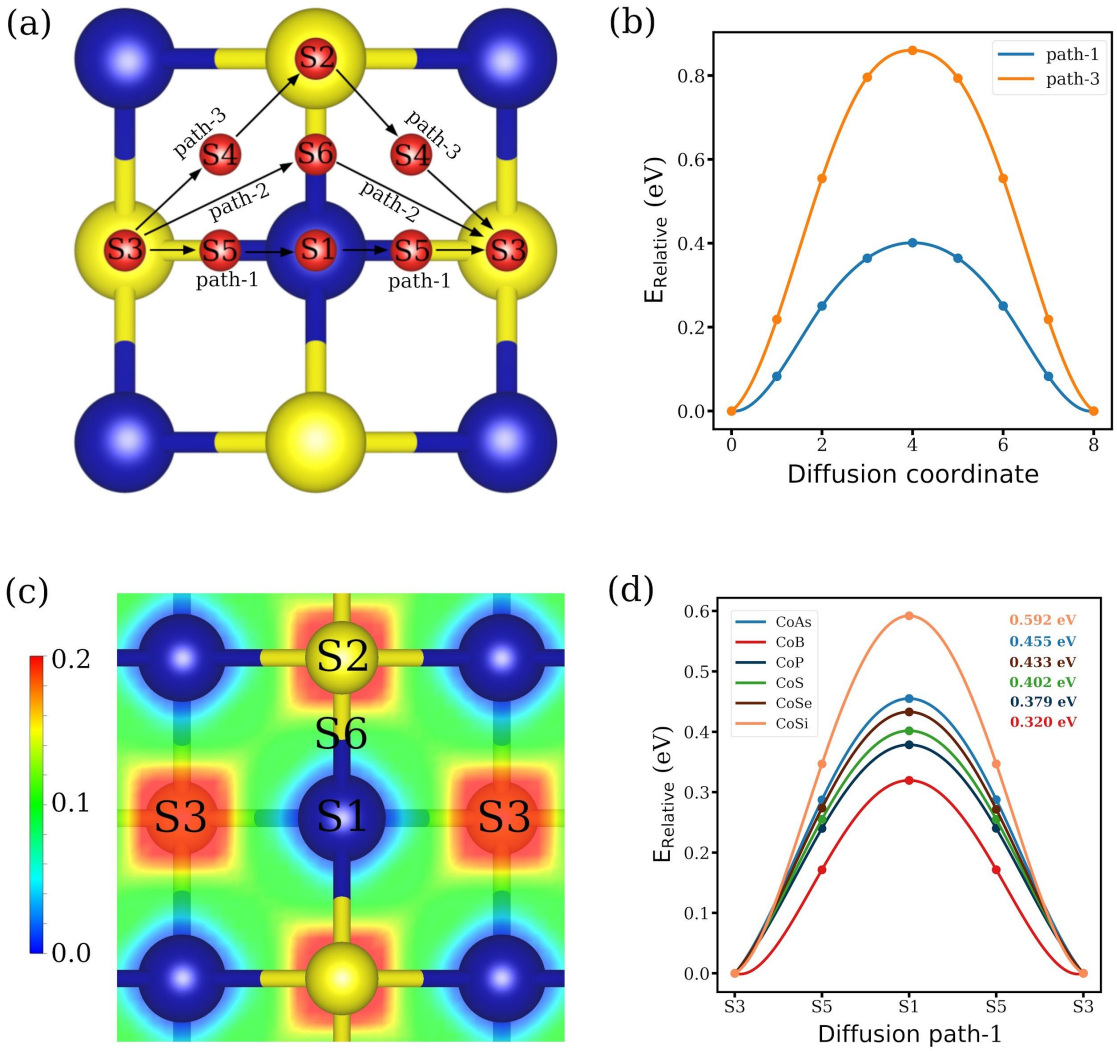

Figure 4. (a) The three different possible paths for a Na atom diffusion on a CoS surface. (b) The migration energy barrier (MEB) values for a Na atom diffusion on a CoS along path-1 and path-3. See text for the results on path-2. (c) ELF plots along the (001) plane of the CoS surface. Cyan and blue (yellow and red) colors depict the regions of low (high) electron density. A sodium atom experiences a low MEB when it moves through the regions of low electron density (path-1). (d) MEBs for a Na atom on all the anti-MXene surfaces along path-1.

In **Figure 4d**, we presented the MEBs for a Na atom on all the anti-MXenes along path-1. The corresponding MEB values for CoAs, CoB, CoP, CoS, CoSe, and CoSi surfaces are 0.46 eV, 0.32 eV, 0.38 eV, 0.4 eV, 0.43 eV, and 0.59 eV, respectively. Since the diffusion barriers of these materials (~ 0.3-0.6 eV) are low compared to the diffusion barriers in commercial Li-graphite batteries (0.45-1.20 eV),[43,44] anti-MXenes are expected to provide excellent rate performance. Also, these diffusion barriers are comparable to the barriers predicted on MXene and various other anode materials. For example, MEB values for Na ion diffusion on $M_3C_2O_2$ MXenes, the MEB values are 0.3 eV (for M = Ti),[23] and 0.36 eV (for M = Hf)[45], etc. On β_{12} and χ_3-borophenes are 0.33 and 0.34 eV,[46] respectively. Moreover, these barriers are low compared to the barriers on 2H-MoS_2 (0.68 eV).[22] Together, these results indicate that Co-anti-MXenes are promising anode materials for sodium-ion batteries.

Finally, we want to mention that some of the earlier studies[47] indicate that the inclusion of quantum mechanical effects like zero-point energies and quantum tunneling would further reduce these barriers, as observed in the case of Li-ion diffusion on group-IV monochalcogenides.[48] However, since Na is 3.3 times heavier than Li, we are expecting only minor changes in its diffusion barrier with the inclusion of such quantum mechanical effects. Since a careful analysis is required to understand the quantum mechanical effects on the Na-ion diffusion behavior, we will consider it in a later study. It should be noted that if at all there is any reduction in diffusion barrier, it is beneficial for the battery (as ions can now move freely on the anode surface and enhance the charge/discharge kinetics).

Multi-layer Sodium Adsorption

Inspired by the encouraging results for a *single* Na atom adsorption and diffusion, we inspected the performance of Co-anti-MXenes for *multiple* sodium atoms adsorption. First, as shown in **Figure S5**, we verified that all Co-anti-MXenes would retain their metallicity even after adsorbing one layer of Na atoms (which suggests that we could adsorb more sodium atoms on these materials). Next, we calculated the adsorption energies for loading multiple layers of sodium atoms on the CoX surfaces. The process of adsorbing multiple layers of sodium atoms at an anode surface (which occurs during a cell charging) can be described using the following equilibrium reaction

$$Na_mCo_2X_2 + (n - m)Na^+ + (n - m)e^- \leftrightharpoons Na_nCo_2X_2$$

where m is the number of Na atoms that are already adsorbed on a CoX surface, (n - m) is the number of Na atoms that are newly added to the surface, and n is the total number of Na atoms on the CoX surface at the end of the adsorption process. Using the above reaction, we can calculate the average adsorption energy per sodium atom for loading the L^{th} layer of sodium atoms on a CoX surface with L-1 layers of sodium atoms as

$$\Delta E^L_{ads.} = [E(Na_nCo_2X_2) - E(Na_mCo_2X_2) - (n - m)*E(Na)] / (n - m)$$

where $E(Na_nCo_2X_2)$ and $E(Na_mCo_2X_2)$ are the energies of CoX surfaces with L and L-1 layers (or n and m number) of sodium atoms, respectively, and E(Na) is the energy of a single Na atom in its bcc bulk. As such, positive adsorption energy at the L^{th} layer (i.e., $\Delta E^L_{ads.} \geq 0$) indicates that adsorbing Na atoms beyond $(L\text{-}1)^{th}$ layer is thermodynamically *not* feasible. Similarly, negative adsorption energy indicates a thermodynamically favorable process. However, care should be taken when the adsorption energy of the L^{th} layer is more negative than the $(L\text{-}1)^{th}$ layer, which indicates the stronger interaction between Na atoms leading to their precipitation and eventual formation of dendrites (Na metal),[49] which are detrimental for battery applications. In all those cases, one should not load beyond the $(L\text{-}1)^{th}$ layer.

In **Table 2**, we provided the layer-wise average adsorption energy values for all CoX surfaces. Here, for each layer, we adsorbed sodium atoms on both sides of the CoX surface. Accordingly, the first-layer loading corresponds to the adsorption of two sodium atoms (one on each side) on a 1×1 CoX surface, the second-layer loading corresponds to the adsorption of four sodium atoms (two on each side), and so on. As shown in **Table 2**, the adsorption energy for loading the 3rd layer of sodium atoms on CoAs and CoP is negative but close to zero. So, on CoAs and CoP, we can load up to a maximum of three layers of sodium atoms. On CoB, CoSe, and CoSi, the adsorption energies for loading four, four, and three layers of sodium atoms, respectively, are more negative than the corresponding energies for loading a layer less. As such, these results suggest that on CoB, CoSe, and CoSi we can load a maximum of three, three, and two layers of sodium, respectively. On CoS, the adsorption values for both the fourth and fifth layers are the same. So, we can load up to four layers of sodium on CoS. The optimized geometries of all CoX surfaces along with the maximum number of sodium atoms that can be adsorbed on them are shown in **Figure S6**. At maximum adsorption, the chemical formulas of these anti-MXenes are $Na_6Co_2As_2$, $Na_6Co_2B_2$, $Na_6Co_2P_2$, $Na_8Co_2S_2$, $Na_6Co_2Se_2$, and $Na_4Co_2Si_2$. As such, except CoSi, *all Co-anti-MXenes can hold up to three sodium atoms per CoX formula unit,* which is much higher than the storage capacity of an amorphous carbon anode (5 Na atoms per 64 C atoms).[50]

Table 2. Average sodiation voltage (V), maximum specific charge capacity (mAh/g), and layer-wise average adsorption energies (eV) of Na atoms on various CoX surfaces. Here, $\Delta E^{L1}_{ads,}$ $\Delta E^{L2}_{ads,}$ etc. correspond to the average adsorption energies for loading one, two, etc. layers of Na atoms on both sides of the CoX surface. The entries of average adsorption energy with the maximum number of sodium atoms adsorbed onto each CoX system (without leading to a dendrite formation) are shown in bold.

System	$\Delta E^{L1}_{ads.}$ (eV)	$\Delta E^{L2}_{ads.}$ (eV)	$\Delta E^{L3}_{ads.}$ (eV)	$\Delta E^{L4}_{ads.}$ (eV)	$\Delta E^{L5}_{ads.}$ (eV)	Avg. Sodiation voltage (V)	Max. Sp. Capacity (mAh/g)
CoAs	-0.730	-0.126	**-0.005**	-0.021	NA	0.287	396.424
CoB	-1.107	-0.074	**-0.006**	-0.014	NA	0.396	579.649
CoP	-0.906	-0.116	**-0.001**	-0.023	NA	0.341	506.082
CoS	-0.679	-0.077	-0.022	**-0.018**	-0.017	0.199	585.978
CoSe	-0.590	-0.060	**-0.015**	-0.017	NA	0.222	388.665
CoSi	-1.265	**-0.016**	-0.115	NA	NA	0.641	403.037

Specific Charge Capacity and Sodiation Voltage

Next, we studied two key electrochemical parameters of an anode material, namely, sodiation voltage and specific charge capacity. Here, sodiation voltage gives us the potential difference between the anode material of our interest and the sodium-metal anode, and the specific charge capacity gives us the amount of charge an anode material can hold per gram (given in mAh/g). Since a sodium atom should reduce the anode material of our interest during the discharge process, the reduction potential of the anode material should be higher than the reduction potential of the Na^+/Na pair (~ -2.71 eV). Also, since the "total cell-voltage" = "cathodic-voltage" - "anodic-voltage", to obtain larger cell voltages, the anodic voltage should be as small as possible (i.e., the reduction potential of the anode material should be as close to the reduction potential of Na^+/Na pair). *As such, a good anode material should have high specific charge capacity and low sodiation voltage*.

Sodiation voltage can be obtained from the Nernst equation, $V = -\Delta G/nF$, where using the second law of thermodynamics, we have $\Delta G = \Delta E + p\Delta V - T\Delta S$. Since the volume and entropy changes during the sodiation process are quite small, we can neglect the volume (ΔV) and entropy (ΔS) terms.[51,52] So the sodiation voltage can be approximated as $V \approx -\Delta E^{L}_{ads.}/z|e|$, where 'z' is the valence charge of the adsorbed metal atom (here for Na, z = 1), and 'e' is the charge of an electron (-1.602×10^{-19} C). As shown in **Figure 5a**, with an increase in the sodium atom concentration, sodiation voltage decreases gradually and it finally reaches close to zero. The average sodiation voltages of CoAs, CoB, CoP, CoS, CoSe, and CoSi are 0.29, 0.40, 0.34, 0.20, 0.22, and 0.64 V, respectively. Apparently, the voltage range (0.2–0.64 V) for all the Co-anti-MXene materials is quite small and when combined with a suitable cathode of ~ 4 V with respect to metallic Na, we can obtain an overall cell voltage of around 3.36–3.8 V (which is within the desirable voltage of 3–3.8 V for a commercial sodium battery).[53–55] It is interesting to note that the sodiation voltage values of anti-MXenes are lower when compared to many known MXene materials like $Ti_3N_2O_2$ (0.721 V),[56] V_2C (0.52 V),[57] Mn_2C (0.8 V),[57] MoC (0.8 V)[58], etc.

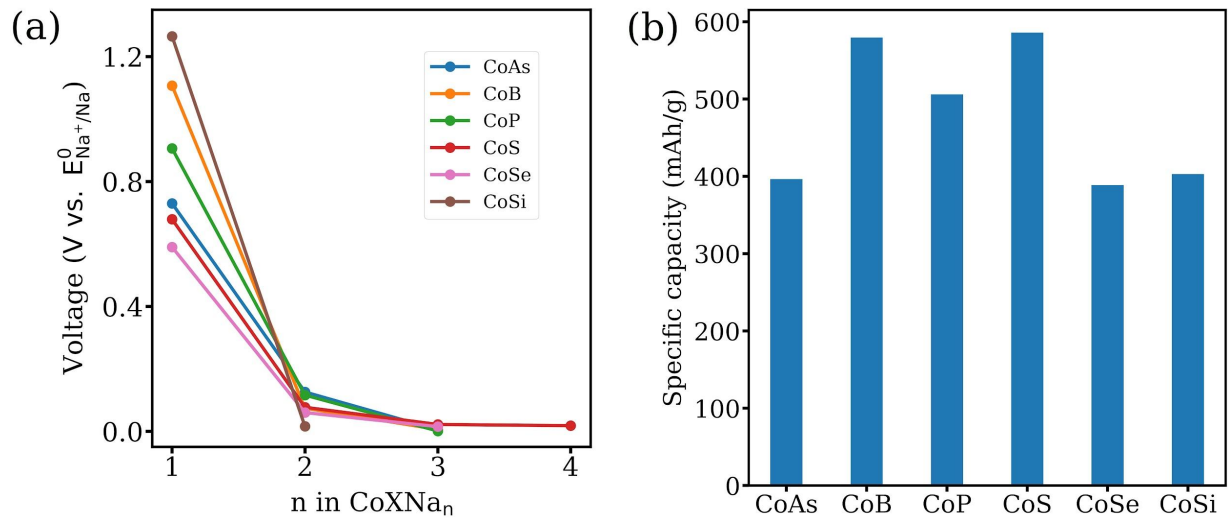

Figure 5. (a) Variation in sodiation voltage with an increase in the concentration of adsorbed sodium atoms on each CoX surface (b) Maximum theoretical specific charge capacity (SCC) of all Co-anti-MXenes. CoS, CoB, and CoP exhibited the highest SCC values, and CoS has the least average sodiation voltage.

The specific charge capacity (SCC) of a Co-anti-MXene material is estimated as C = nzF/M(Na_nCoX), where 'n' is the number of Na atoms adsorbed per formula unit of CoX anti-MXene, 'z' is the valence of the adsorbed metal atom (for Na, z = 1), 'F' is the Faraday constant (26801.486 mAh/mol), and 'M(Na_nCoX)' is the molecular weight of the active materials that participate in the electrochemical reaction.[59] Since z and F constants for all the systems in the current study, SCC only varies with respect to the number of atoms and the molecular weight. Moreover, for a fixed 'n', SCC will be the highest for systems that are lightweight, and for systems with roughly the same weight, a system with the highest number of Na atoms would give the highest SCC.

Among the six Co-anti-MXenes, CoAs, CoB, CoP, and CoSe have the same (three) number of sodium atoms adsorbed per formula unit. However, their SCC values are different due to the differences in the atomic weights of the non-metal atoms. Since Boron is the lightest non-metal atom, CoB provides the maximum SCC (~580 mAh/g), and CoSe gives the minimum SCC (~389 mAh/g) because Se is the heaviest atom among the four. Similarly, although CoSi accommodates only two Na atoms per formula unit, its SCC slightly exceeds that of the CoAS and CoSe (which hold three Na atoms per formula unit) because of the lower atomic weight of Si than As and Se. Of all the six anti-MXenes, CoS holds the maximum number of Na atoms (four Na atoms per formula unit) and it provides the highest SCC (586 mAh/g) among all. As such, CoB and CoS provide the best SCC values and are superior to various other 2D materials that are proposed as anode candidates for NIBs. Examples include, ReS_2 (428 mAh/g),[60] FeSe anti-MXene (473 mAh/g),[61] MXenes like $Ti_3C_2O_2$ (536 mAh/g),[62] $V_3C_2O_2$ (513.5 mAh/g),[63] etc. The other CoX anti-MXenes (X = As, P, Se, and Si) also show better or similar SCC values when compared to MoS_2 (146 mAh/g),[22] Sc_2C (362 mAh/g),[64] and M_2C MXenes (190-288 mAh/g) for M = Ti, V, Cr, Mn, and Mo,[57] etc.

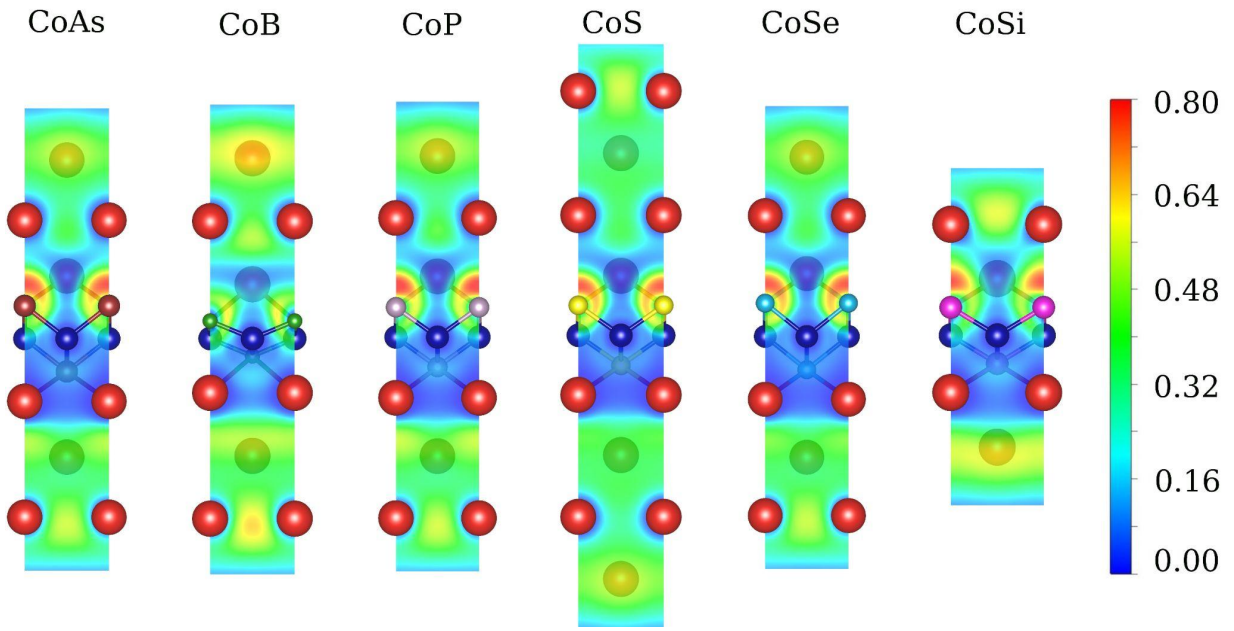

Figure 6. Electron localization functions projected along the (010) planes of $Na_6Co_2As_2$, $Na_6Co_2B_2$, $Na_6Co_2P_2$, $Na_8Co_2S_2$, $Na_6Co_2Se_2$, and $Na_4Co_2Si_2$.

To understand the stability of the CoX structures with multiple layers of Na atoms adsorbed onto them, we analyzed the electron localization functions (ELFs) projected along the (010) plane. As shown in **Figure 6**, in all cases, electron localization is more (red and yellow color regions, 0.6 ≤ ELF ≤ 0.8) between the non-metal (X) atoms and the first layer of Na atoms, indicating a stronger ionic interaction between them. The ionic interaction between the first layer of Na atoms and X atoms can also be seen in the Bader charge analysis (c.f. **Table 1**), where a positive charge (> +0.5 e) is observed on Na atoms at the S3 site. Above the first layer of Na atoms, electrons are primarily localized between the sodium atoms (greenish-yellow color regions, 0.4 ≤ ELF ≤ 0.56), which reduces both the interlayer and intralayer Na-Na repulsion and stabilizes multiple layers of Na atoms on these Co-anti-MXenes.[23,62]

Finally, we studied the deformation in maximally sodiated structures of all Co-anti-MXenes. It is apparent that a good anode material should show minimum deformation (i.e., it should retain its original structure) even after a large number of charge/discharge cycles.[65] To examine the cyclability of the anti-Mxenes, we measured the differences in the anti-MXene thickness and total energy of the CoX surfaces before and after loading multiple layers of sodium atoms. These results are summarized in **Figure S7**, and they clearly suggest that all materials deform very little (< 10 % layer thickness and < 0.1 eV).[65]

We have also examined the thermal stability of the maximally sodiated Co-anti-MXenes. For these simulations, we only considered the anti-MXenes that exhibited the maximum SCC

(CoB, CoP, and CoS). As shown in **Figure 7**, all the maximally sodiated Co-anti-MXenes (with the compound formulae Na_3CoB, Na_3CoP, and Na_4CoS) are stable at 300 K; we did not observe any agglomeration of sodium atoms or any appreciable structural distortions in the CoX surfaces during the 15 ps simulation period. Moreover, the energy fluctuations during the simulation period are also very small (~ 0.5 eV) for all the systems. From these results, we can conclude that the Co-anti-MXenes are thermally stable even after adsorbing the maximum number of sodium atoms.

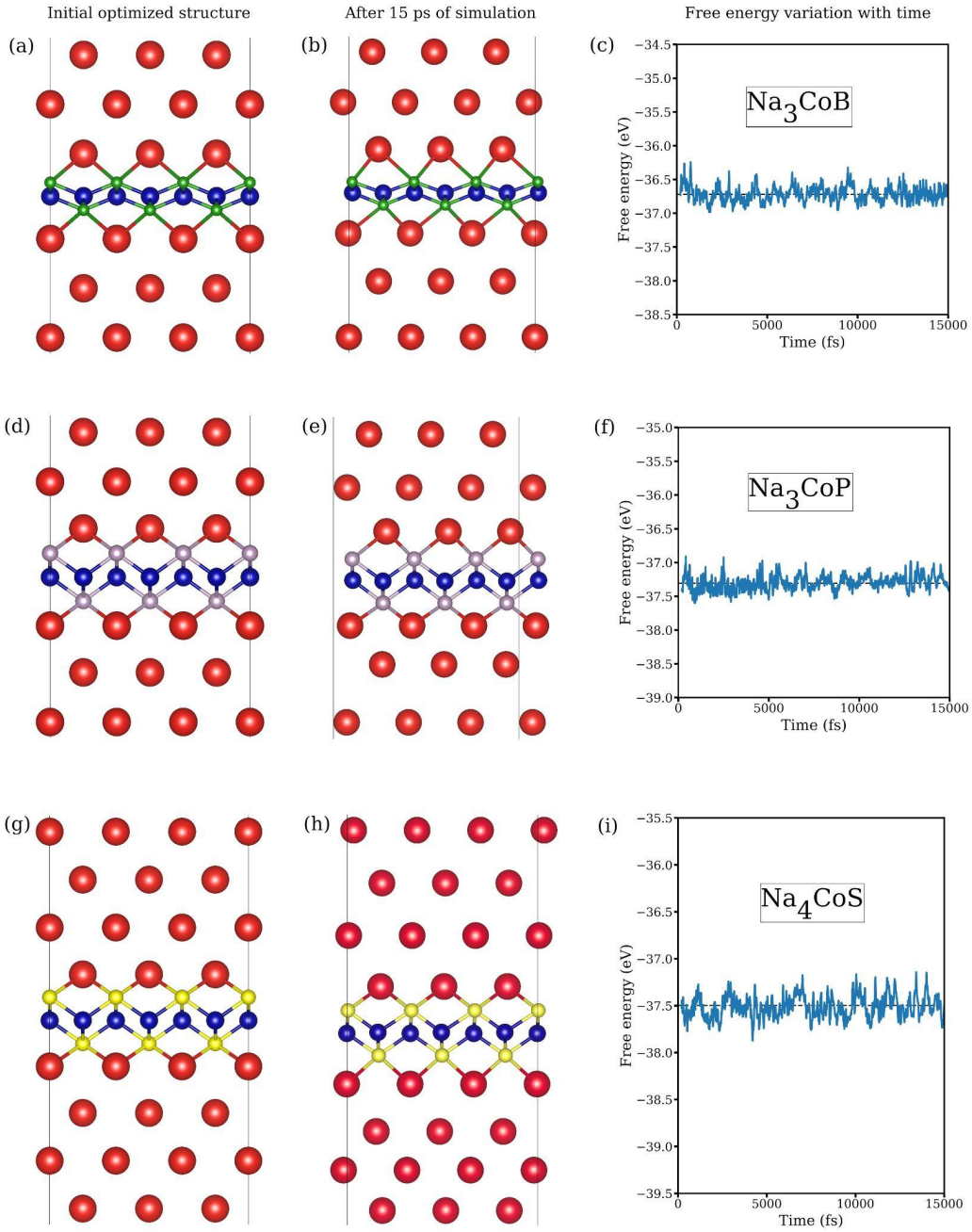

Figure 7. (a), (d), and (g) depict the optimized structures of Na_3CoB, Na_3CoP, and Na_4CoS systems, respectively, at the 0th ps of the simulation. (b), (e), and (h) depict the corresponding structures after a 15 ps NVT simulation. (c), (f), and (i) show the free energy fluctuations of Na_3CoB, Na_3CoP, and Na_4CoS during the 15 ps AIMD simulation at 300 K.

We also studied the expansion of anti-MXenes along the z-axis (only for the CoS system) after the sodium adsorption.[66] Since the interlayer spacing in Co-anti-MXenes is not available experimentally, we performed cell optimizations of the “CoS bilayer", and find the value to be 3.155 Å. After intercalating with a single layer of sodium atoms, the interlayer separation only increased by 0.86%, i.e., to 3.18 Å, as shown in **Figure S8**. This expansion is much lower than the 40% thickness expansion observed in graphite after single layer sodium adsorption.[67] After four layers of Na adsorption, the interlayer separation in CoS anti-MXene increased to 11.556 Å, corresponding to an expansion of 266% (shown in **Figure S8**), which is comparable to the ~268% expansion observed in $Ti3N_2O_2$ MXene bilayers[68] after five-layer Na adsorption, and many other 2D-materials.[68–73] Therefore, it can be concluded that the thickness expansion of anti-MXenes is similar to that of the other MXene materials that are proposed for battery applications and is negligible compared to graphite.

As such, with low sodiation voltages (which in turn give rise to high cell voltages), high specific charge capacities, and low deformation, most of the Co-anti-MXenes are suitable anode candidates for designing high energy-density (= specific charge capacity × cell voltage) sodium-ion batteries.

Conclusions

In summary, we systematically examined six novel cobalt anti-MXenes, namely, CoAs, CoB, CoP, CoS, CoSe, and CoSi, as plausible anode candidates for the sodium-ion batteries (NIBs). To this end, we computed various physical and electrochemical properties of these materials, such as binding energy, specific charge capacity, sodiation voltage, etc., using density functional theory calculations. Single Na atom binding energies on these metallic materials range from -0.55 to -1.16 eV, suggesting strong physisorption of a Na atom on Co-anti-MXenes. As revealed by the charge density difference maps and Bader charge analysis, such strong physisorption arises because the Na atom becomes positive after adsorption and shares its electrons with four non-metal atoms. Moreover, both binding a Na atom firmly, and making it positive after adsorption, are desirable properties of good anode material. Also, the reasonably low diffusion energy barriers (range from 0.32–0.59 eV) for Na atoms on Co-anti-MXenes imply high charge/discharge rates in battery applications.

As expected, the average adsorption energies decreased with an increase in the Na atom concentration, but intercalation remained favorable until two to four Na atoms per formula unit. Indeed, the specific charge capacities of the Co-anti-MXenes lie in the range of ~ 390–590 mAh/g, which is higher than many well-studied anode materials. Moreover, except CoSi, the

average sodiation voltage of all the Co-anti-MXenes is quite low (< 0.4 V). Altogether, these results lead us to conclude that the Co-anti-MXenes are promising anode materials for low-cost Na-ion battery applications and further encourage us to explore other anti-MXene materials for various battery applications.

Supporting Information

Optimized structures of all Co-anti-MXenes; structural parameters, and ELF plots of Co-anti-MXenes; Co-PDOS in pristine Co-anti-MXenes; CDD plots of Na adsorption; PDOS of CoX-anti-MXenes after Na atom adsorption; Maximum Na layers loaded structures on CoX; and Structural Deformation in Co-anti-MXenes.

Acknowledgments

We thank Dr. Jinxing Gu and Prof. Zhongfang Chen for several fruitful discussions. SKR acknowledges the National Supercomputing Mission (NSM) for providing computing resources of 'PARAM Shakti' at IIT Kharagpur, which is implemented by C-DAC and supported by the Ministry of Electronics and Information Technology (MeitY) and Department of Science and Technology (DST), Government of India. S. S. R. K. C. Y. acknowledges the financial support of IIT Madras through its new faculty support grants NFSG (IP2021/0972CY/NFSC008973) and NFIG (RF2021/0577CY/NFIG008973), and DST-SERB (SRG/2021/001455).

References

(1) Perveen, T.; Siddiq, M.; Shahzad, N.; Ihsan, R.; Ahmad, A.; Shahzad, M. I. Prospects in Anode Materials for Sodium-Ion Batteries - A Review. *Ren. Sus. Ener. Rev*. **2020**, 119, 109549.
(2) Haas, O.; Cairns, E. J. Chapter 6. Electrochemical Energy Storage. *Annu. Rep. Prog. Chem. Sect. C: Phys. Chem.* **1999**, *95* (0), 163–198.
(3) Neumann, J.; Petranikova, M.; Meeus, M.; Gamarra, J. D.; Younesi, R.; Winter, M.; Nowak, S. Recycling of Lithium‐Ion Batteries—Current State of the Art, Circular Economy, and Next Generation Recycling. *Adv. Ener. Mater*. **2022**, 12, 2102917.
(4) Baum, Z. J.; Bird, R. E.; Yu, X.; Ma, J. Lithium-Ion Battery Recycling─Overview of Techniques and Trends. *ACS Energy Letters*. **2022**, 7, 712–719.
(5) Yabuuchi, N.; Kubota, K.; Dahbi, M.; Komaba, S. Research Development on Sodium-Ion Batteries. *Chem. Rev.* **2014**, 114 (23), 11636–11682.
(6) Yamijala, S. S. R. K. C.; Kwon, H.; Guo, J.; Wong, B. M. Stability of Calcium Ion Battery Electrolytes: Predictions from Ab Initio Molecular Dynamics Simulations. *ACS Appl. Mater. Interfaces* **2021**, 13 (11), 13114–13122.
(7) Marzouk, A.; Balbuena, P. B.; El-Mellouhi, F. Open Framework Allotropes of Silicon: Potential Anode Materials for Na and Li-Ion Batteries. *Electrochimica Acta*. **2016**, 207,

301–307.
(8) Geng, L.; Scheifers, J. P.; Fu, C.; Zhang, J.; Fokwa, B. P. T.; Guo, J. Titanium Sulfides as Intercalation-Type Cathode Materials for Rechargeable Aluminum Batteries. *ACS Appl. Mater. Interfaces* **2017**, 9 (25), 21251–21257.
(9) Chowdhury, C.; Gain, P.; Datta, A. Evolutionary Structure Prediction-Assisted Design of Anode Materials for Ca-Ion Battery Based on Phosphorene. *Phys. Chem. Chem. Phys.* **2021**, *23* (15), 9466–9475.
(10) Sada, K.; Gond, R.; Bothra, N.; Pati, S. K.; Barpanda, P. Potassium Cobalt Pyrophosphate as a Nonprecious Bifunctional Electrocatalyst for Zinc-Air Batteries. *ACS Appl. Mater. Interfaces*. **2022**, 14, 8992–9001.
(11) Mishra, S. B.; Abhijitha, V. G.; Ramaprabhu, S.; Nanda, B. R. K. Graphdiyne—A Two-Dimensional Cathode for Aluminum Dual-Ion Batteries with High Specific Capacity and Diffusivity. *ACS Appl. Energy Mater*. **2021**, 4, 7786–7799.
(12) Panigrahi, P.; Mishra, S. B.; Hussain, T.; Nanda, B. R. K.; Ahuja, R. Density Functional Theory Studies of Si_2BN Nanosheets as Anode Materials for Magnesium-Ion Batteries. *ACS Appl. Nano Mater*. **2020**, 3, 9055–9063.
(13) Sawicki, M.; Shaw, L. L. Advances and Challenges of Sodium-Ion Batteries as Post Lithium-Ion Batteries. *RSC Adv*., **2015**, 5, 53129–53154.
(14) Xiao, J.; Li, X.; Tang, K.; Wang, D.; Long, M.; Gao, H.; Chen, W.; Liu, C.; Liu, H.; Wang, G. Recent Progress of Emerging Cathode Materials for Sodium-Ion Batteries. *Mater. Chem. Front.,* **2021**, 5 (10), 3735–3764.
(15) Wen, Y.; He, K.; Zhu, Y.; Han, F.; Xu, Y.; Matsuda, I.; Ishii, Y.; Cumings, J.; Wang, C. Expanded Graphite as Superior Anode for Sodium-Ion Batteries. *Nat. Commun.* **2014**, 5, 4033.
(16) Wu, E. A.; Banerjee, S.; Tang, H.; Richardson, P. M.; Doux, J.-M.; Qi, J.; Zhu, Z.; Grenier, A.; Li, Y.; Zhao, E.; Deysher, G.; Sebti, E.; Nguyen, H.; Stephens, R.; Verbist, G.; Chapman, K. W.; Clément, R. J.; Banerjee, A.; Meng, Y. S.; Ong, S. P. A Stable Cathode-Solid Electrolyte Composite for High-Voltage, Long-Cycle-Life Solid-State Sodium-Ion Batteries. *Nat. Commun.* **2021**, *12* (1), 1256.
(17) Chowdhury, C.; Karmakar, S.; Datta, A. Capping Black Phosphorene by H-BN Enhances Performances in Anodes for Li and Na Ion Batteries. *ACS Energy Lett*. **2016**, 1, 253–259.
(18) Mazumder, M.; Pati, S. K. Theoretical Insights into $Na_5M(PO_4)_2F_2$ (M = Cr, V): A Fluorophosphate-Based High-Performance Cathode System for Sodium-Ion Batteries. *J. Phys. Chem. C* **2021**, *125* (36), 19593–19599.
(19) Ghosh, S.; Barman, N.; Gonzalez-Correa, E.; Mazumder, M.; Zaveri, A.; Giovine, R.; Manche, A.; Pati, S. K.; Clément, R. J.; Senguttuvan, P. Elucidating the Impact of Mg Substitution on the Properties of NASICON-$Na_{3+Y}V_{2-Y}Mg_Y(PO_4)_3$ Cathodes. *Adv. Funct. Mater.* **2021**, *31* (48), 2105463.
(20) Gu, J.; Zhao, Z.; Huang, J.; Sumpter, B. G.; Chen, Z. MX Anti-MXenes from Non-van Der Waals Bulks for Electrochemical Applications: The Merit of Metallicity and Active Basal Plane. *ACS Nano* **2021**, *15* (4), 6233–6242.
(21) Ge, P.; Fouletie M. Electrochemical Intercalation of Sodium in Graphite. *Solid State Ionics*. **1988**, 28-30, 1172–1175.
(22) Mortazavi, M.; Wang, C.; Deng, J.; Shenoy, V. B.; Medhekar, N. V. Ab Initio Characterization of Layered MoS_2 as Anode for Sodium-Ion Batteries. *J. Power Sources* **2014**, 268, 279–286.
(23) Xie, Y.; Dall'Agnese, Y.; Naguib, M.; Gogotsi, Y.; Barsoum, M. W.; Zhuang, H. L.; Kent, P. R. C. Prediction and Characterization of MXene Nanosheet Anodes for Non-Lithium-Ion Batteries. *ACS Nano* **2014**, 8 (9), 9606–9615.
(24) Kresse, G.; Furthmüller, J. Efficient Iterative Schemes for Ab Initio Total-Energy Calculations Using a Plane-Wave Basis Set. *Phys. Rev. B Condens. Matter* **1996**, 54 (16),

11169–11186.
(25) Blöchl, P. E. Projector Augmented-Wave Method. *Physical Review B*. **1994**, 50, 17953–17979.
(26) Kresse, G.; Joubert, D. From Ultrasoft Pseudopotentials to the Projector Augmented-Wave Method. *Physical Review B*. **1999**, 59, 1758–1775.
(27) Perdew, J. P.; Burke, K.; Ernzerhof, M. Generalized Gradient Approximation Made Simple. *Phys. Rev. Lett*. **1996**, 77, 3865–3868.
(28) Grimme, S.; Ehrlich, S.; Goerigk, L. Effect of the Damping Function in Dispersion Corrected Density Functional Theory. *J. Comput. Chem.* **2011**, *32* (7), 1456–1465.
(29) Monkhorst, H. J.; Pack, J. D. Special Points for Brillouin-Zone Integrations. *Phys. Rev. B* **1976**, 13, 5188–5192.
(30) Henkelman, G.; Uberuaga, B. P.; Jónsson, H. A Climbing Image Nudged Elastic Band Method for Finding Saddle Points and Minimum Energy Paths. *J. Chem. Phys*. **2000**, 113, 9901–9904.
(31) Wang, V.; Xu, N.; Liu, J.-C.; Tang, G.; Geng, W.-T. VASPKIT: A User-Friendly Interface Facilitating High-Throughput Computing and Analysis Using VASP Code. *Computer Physics Communications*. **2021**, 267, 108033.
(32) Ong, S. P.; Richards, W. D.; Jain, A.; Hautier, G.; Kocher, M.; Cholia, S.; Gunter, D.; Chevrier, V. L.; Persson, K. A.; Ceder, G. Python Materials Genomics (pymatgen): A Robust, Open-Source Python Library for Materials Analysis. *Comput. Mater. Sci.* **2013**, *68*, 314–319.
(33) Momma, K.; Izumi, F. VESTA: A Three-Dimensional Visualization System for Electronic and Structural Analysis. *J. Appl. Crystallogr.* **2008**, 41 (3), 653–658.
(34) Králik, M. Adsorption, Chemisorption, and Catalysis. *Chem. Pap.* **2014**, *68* (12), 1625−1638.
(35) Ma, P.; Fang, D.; Liu, Y.; Shang, Y.; Shi, Y.; Yang, H. Y. MXene-Based Materials for Electrochemical Sodium-Ion Storage. *Adv. Sci.* **2021**, 8 (11), 2003185.
(36) Wang, X.; Shen, X.; Gao, Y.; Wang, Z.; Yu, R.; Chen, L. Atomic-Scale Recognition of Surface Structure and Intercalation Mechanism of Ti_3C_2X. *J. Am. Chem. Soc.* **2015**, *137* (7), 2715–2721.
(37) Dall'Agnese, Y.; Taberna, P.-L.; Gogotsi, Y.; Simon, P. Two-Dimensional Vanadium Carbide (MXene) as Positive Electrode for Sodium-Ion Capacitors. *J. Phys. Chem. Lett.* **2015**, *6* (12), 2305–2309.
(38) Zhou, J.; Zha, X.; Zhou, X.; Chen, F.; Gao, G.; Wang, S.; Shen, C.; Chen, T.; Zhi, C.; Eklund, P.; Du, S.; Xue, J.; Shi, W.; Chai, Z.; Huang, Q. Synthesis and Electrochemical Properties of Two-Dimensional Hafnium Carbide. *ACS Nano* **2017**, 11 (4), 3841–3850.
(39) Dawson, J. A.; Robertson, J. Improved Calculation of Li and Na Intercalation Properties in Anatase, Rutile, and TiO_2(B). *The Journal of Physical Chemistry C*. **2016**, 120 (40), 22910–22917.
(40) Lan, T.; Wang, T.; Zhang, W.; Wu, N.-L.; Wei, M. Rutile TiO_2 Mesocrystals with Tunable Subunits as a Long-Term Cycling Performance Anode for Sodium-Ion Batteries. *Journal of Alloys and Compounds* **2017**, 699, 455-462.
(41) Song, D.-X.; Xie, L.; Zhang, Y.-F.; Lu, Y.; An, M.; Ma, W.-G.; Zhang, X. Multilayer Ion Load and Diffusion on TMD/MXene Heterostructure Anodes for Alkali-Ion Batteries. *ACS Appl. Energy Mater*. **2020**, 3 (8), 7699–7709.
(42) Acerce, M.; Voiry, D.; Chhowalla, M. Metallic 1T Phase MoS_2 Nanosheets as Supercapacitor Electrode Materials. *Nat. Nanotechnology* **2015**, 10 (4), 313–318.
(43) Ganesh, P.; Kim, J.; Park, C.; Yoon, M.; Reboredo, F. A.; Kent, P. R. C. Binding and Diffusion of Lithium in Graphite: Quantum Monte Carlo Benchmarks and Validation of van Der Waals Density Functional Methods. *J. Chem. Theory. Comp*. **2014**, 10 (12), 5318–5323.

(44) Toyoura, K.; Koyama, Y.; Kuwabara, A.; Oba, F.; Tanaka, I. First-Principles Approach to Chemical Diffusion of Lithium Atoms in a Graphite Intercalation Compound. *Phys. Rev. B*. **2008**, 78 (21), 214303.
(45) Li, N.; Li, Y.; Zhu, X.; Huang, C.; Kai, J.-J.; Fan, J. Theoretical Investigation of the Structure–property Correlation of MXenes as Anode Materials for Alkali Metal Ion Batteries. *J. Phys. Chem. C* **2020**, 124 (28), 14978–14986.
(46) Zhang, X.; Hu, J.; Cheng, Y.; Yang, H. Y.; Yao, Y.; Yang, S. A. Borophene as an Extremely High Capacity Electrode Material for Li-Ion and Na-Ion Batteries. *Nanoscale* **2016**, *8* (33), 15340–15347.
(47) Karmakar, S.; Datta, A. Role of Heavy Atom Tunneling in Myers-Saito Cyclization of Cyclic Enyne-Cumulene Systems. *J. Phys. Chem. B* **2016**, *120* (5), 945–950.
(48) Karmakar, S.; Chowdhury, C.; Datta, A. Two-Dimensional Group IV Monochalcogenides: Anode Materials for Li-Ion Batteries. *J. Phys. Chem. C* **2016**, *120* (27), 14522–14530.
(49) Yang, Z.; Zheng, Y.; Li, W.; Zhang, J. Tuning the Electrochemical Performance of Ti_3C_2 and Hf_3C_2 Monolayer by Functional Groups for Metal-Ion Battery Applications. *Nanoscale* **2021**, *13* (26), 11534–11543.
(50) Legrain, F.; Sottmann, J.; Kotsis, K.; Gorantla, S.; Sartori, S.; Manzhos, S. Amorphous (Glassy) Carbon, a Promising Material for Sodium Ion Battery Anodes: A Combined First-Principles and Experimental Study. *The Journal of Phys. Chem. C* **2015,** 119 (24), 13496–13501.
(51) Aydinol, M. K.; Kohan, A. F.; Ceder, G.; Cho, K.; Joannopoulos, J. Ab Initiostudy of Lithium Intercalation in Metal Oxides and Metal Dichalcogenides. *Phys. Rev. B* **1997**, 56 (3), 1354–1365.
(52) Ma, Y. Computer Simulation of Cathode Materials for Lithium Ion and Lithium Batteries: A Review. *Energy & Environmental Materials*. **2018**, 1, 148–173.
(53) Delmas, C,; Braconnier,JJ.; Fouassier,C.; Hagenmuller, P. Electrochemical Intercalation of Sodium in Na_xCoO_2 Bronzes. *Solid State Ionics.* **1981**, *3-4*, 165–169.
(54) Broux, T.; Fauth, F.; Hall, N.; Chatillon, Y.; Bianchini, M.; Bamine, T.; Leriche, J.-B.; Suard, E.; Carlier, D.; Reynier, Y.; Simonin, L.; Masquelier, C.; Croguennec, L. High Rate Performance for Carbon-coated $Na_3V_2(PO_4)_2F_3$ in Na-ion Batteries. *Small Methods* **2019**, *3* (4), 1800215.
(55) Abraham, K. M. How Comparable Are Sodium-Ion Batteries to Lithium-Ion Counterparts? *ACS Energy Letters*. **2020**, 5 (11), 3544–3547.
(56) Yu, H.; Lin, W.; Zhang, Y.; Li, Y.; Ding, K.; Huang, S.; Chen, W. Exploring the Potentials of Ti_3N_2 and $Ti_3N_2X_2$ (X = O, F, OH) Monolayers as Anodes for Li or Non-Li Ion Batteries from First-Principles Calculations. *RSC Advances*. **2019**, 9 (69), 40340–40347.
(57) Yang, E.; Ji, H.; Kim, J.; Kim, H.; Jung, Y. Exploring the Possibilities of Two-Dimensional Transition Metal Carbides as Anode Materials for Sodium Batteries. *Phys. Chem. Chem. Phys.* **2015**, *17* (7), 5000–5005.
(58) Yu, Y.; Guo, Z.; Peng, Q.; Zhou, J.; Sun, Z. Novel Two-Dimensional Molybdenum Carbides as High Capacity Anodes for Lithium/sodium-Ion Batteries. *J. Mater. Chem. A.* **2019**, *7* (19), 12145–12153.
(59) Linden, D.; Linden, of T. N.; Reddy, T.; David, L.; Thomas, R. *Handbook of Batteries*; McGraw-Hill Professional, **2002**.
(60) Mukherjee, S.; Banwait, A.; Grixti, S.; Koratkar, N.; Singh, C. V. Adsorption and Diffusion of Lithium and Sodium on Defective Rhenium Disulfide: A First Principles Study. *ACS Appl. Mater. Interfaces* **2018**, *10* (6), 5373–5384.
(61) Lv, X.; Li, F.; Gong, J.; Gu, J.; Lin, S.; Chen, Z. Metallic FeSe Monolayer as an Anode Material for Li and Non-Li Ion Batteries: A DFT Study. *Phys. Chem. Chem. Phys.* **2020**, *22* (16), 8902–8912.
(62) Li, N.; Li, Y.; Zhu, X.; Huang, C.; Kai, J.-J.; Fan, J. Theoretical Investigation of the

Structure–property Correlation of MXenes as Anode Materials for Alkali Metal Ion Batteries. *J. Phys. Chem. C.* **2020**, *124* (28), 14978–14986.
(63) Fan, K.; Ying, Y.; Li, X.; Luo, X.; Huang, H. Theoretical Investigation of V_3C_2 MXene as Prospective High-Capacity Anode Material for Metal-Ion (Li, Na, K, and Ca) Batteries. *J. Phys. Chem. C.* **2019**, 123 (30), 18207–18214.
(64) Lv, X.; Wei, W.; Sun, Q.; Yu, L.; Huang, B.; Dai, Y. Sc_2C as a Promising Anode Material with High Mobility and Capacity: A First-Principles Study. *ChemPhysChem* **2017**, 18 (12), 1627–1634.
(65) Li, G.; Li, J.-Y.; Yue, F.-S.; Xu, Q.; Zuo, T.-T.; Yin, Y.-X.; Guo, Y.-G. Reducing the Volume Deformation of High Capacity SiOx/G/C Anode toward Industrial Application in High Energy Density Lithium-Ion Batteries. *Nano Energy*. **2019**, 60, 485–492.
(66) Ye, H.; Zhang, Y.; Yin, Y.-X.; Cao, F.-F.; Guo, Y.-G. An Outlook on Low-Volume-Change Lithium Metal Anodes for Long-Life Batteries. *ACS Cent. Sci* **2020**, *6* (5), 661–671.
(67) Lenchuk, O.; Adelhelm, P.; Mollenhauer, D. New Insights into the Origin of Unstable Sodium Graphite Intercalation Compounds. *Phys. Chem. Chem. Phys.* **2019**, 21 (35), 19378–19390.
(68) Zhang, W.; Liu, S.; Chen, J.; Hu, F.; Wang, X.; Huang, H.; Yao, M. Exploring the Potentials of TiCNT (= 0, 1, 2)-MXene for Anode Materials of High-Performance Sodium-Ion Batteries. *ACS Appl. Mater. Interfaces* **2021**, *13* (19), 22341–22350.
(69) Ge, B.; Chen, B.; Li, L. Ternary Transition Metal Chalcogenides Ti_2PX_2 (X = S, Se, Te) Anodes for High Performance Metal-Ion Batteries: A DFT Study. *Appl. Surf. Sci.* **2021**, *550*, 149177.
(70) Zhou, D.; Li, C.; Yin, F.; Tang, X.; Pu, C.; He, C. Two-Dimensional 1T-PS_2 as a Promising Anode Material for Sodium-Ion Batteries with Ultra-High Capacity, Low Average Voltage and Appropriate Mobility. *Chin. Chem. Lett.* **2020**, *31* (9), 2325–2329.
(71) Zhu, C.; Qu, X.; Zhang, M.; Wang, J.; Li, Q.; Geng, Y.; Ma, Y.; Su, Z. Planar NiC_3 as a Reversible Anode Material with High Storage Capacity for Lithium-Ion and Sodium-Ion Batteries. *J. Mater. Chem. A,* **2019**, *7* (21), 13356–13363.
(72) Sharma, A.; Khan, M. S.; Khan, M. S.; Husain, M. Ab Initio Study of Molybdenum Sulfo-Selenides Alloy as a Flexible Anode for Sodium-Ion Batteries. *Appl. Surf. Sci.* **2021**, *536*, 147973.
(73) Yuan, X.; Zhang, Z.; He, Y.; Zhao, S.; Zhou, N. Multilayer Load and Fast Diffusion of Metal Ions on a Ti_2CS_2/blue Phosphorene Heterostructure Anode. *J. Phys. Chem. C.* **2022**, *126* (1), 91–101.

TOC Graphic

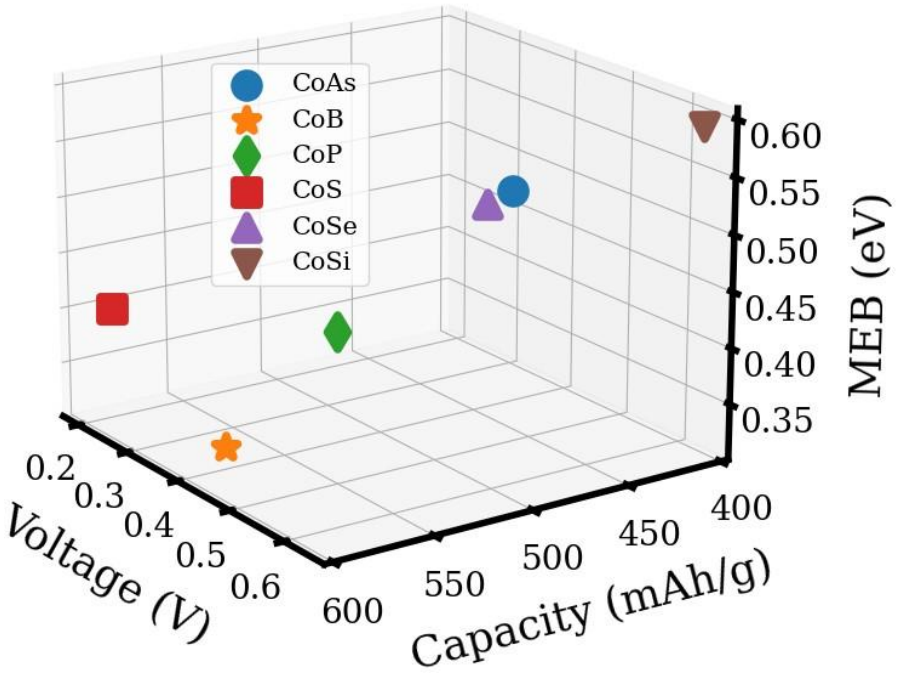
CoAs
CoB
CoP
CoS
CoSe
CoSi
0.60
0.55
0.50
0.45
0.40
0.35
MEB (eV)
0.2
0.3
0.4
0.5
0.6
Voltage (V)
600
550
500
450
400
Capacity (mAh/g)